

Original Research

ARHGAP10, Transcriptionally Regulated by Sodium Butyrate, Promotes Ferroptosis of Ovarian Cancer Cells

Huihui Ke^{1,†}, Juan Shao^{1,†}, Jiachang Hu¹, Xumin Song¹, Hongyu Han¹, Zhanpeng Zhu¹, Xinying Zhou¹, Li Chen^{1,*}, Ying Shan^{1,*}¹Department of Obstetrics and Gynecology, Shanghai Pudong Hospital, Fudan University Pudong Medical Center, 201399 Shanghai, China*Correspondence: chenli8369@163.com (Li Chen); shanshanpx@163.com (Ying Shan)

†These authors contributed equally.

Academic Editor: Sung Eun Kim

Submitted: 13 December 2023 Revised: 21 March 2024 Accepted: 8 April 2024 Published: 28 April 2024

Abstract

Background: Ovarian cancer is a highly lethal gynecologic malignancy. ARHGAP10, a member of Rho GTPase-activating proteins, is a potential tumor suppressor in ovarian cancer. However, its role and the involved mechanism need further examination. Here, we investigated whether ARHGAP10 is also associated with ferroptosis. **Methods:** Lentivirus infection was used for gene overexpression or silencing. Real-time polymerase chain reaction (RT-PCR) and Western blot were used to assess mRNA and protein levels, respectively. Cell viability was assessed by Cell Counting Kit-8 (CCK-8) assay. Lipid reactive oxygen species level was measured by flow cytometry. A tumorigenicity assay was performed to evaluate tumor growth *in vivo*, and sections of mouse tumor tissues were examined by immunofluorescence microscopy. Chromatin Immunoprecipitation (ChIP) assay was used to assess the binding of H3K9ac to the promoter region of ARHGAP10. **Results:** ARHGAP10 overexpression promoted ferroptosis in ovarian cancer cells, resulting in decreased cell viability, and increased lipid reactive oxygen species (ROS) level. Further, it decreased and increased GPX4 and PTGS2 expression, respectively, and also induced suppression of tumor growth in mice. Fer-1, a potent inhibitor of ferroptosis, suppressed the above effects of ARHGAP10. Contrarily, ARHGAP10 silencing alleviated ferroptosis in ovarian cancer cells, which was reversed by RSL3, a ferroptosis-inducing agent. Lastly, sodium butyrate (SB) was found to transcriptionally regulate ARHGAP10, thereby also contributing to the ferroptosis of ovarian cancer cells. **Conclusions:** Our results suggest that SB/ARHGAP10/GPX4 is a new signaling axis involved in inducing ferroptosis in ovarian cancer cells and suppressing tumor growth, which has potential clinical significance.

Keywords: ovarian cancer; ARHGAP10; sodium butyrate; ferroptosis

1. Introduction

Ovarian cancer is the second most common and fatal gynecologic malignancy [1]. There is a paucity of effective screening methods for ovarian cancer. Owing to the nonspecific symptoms in the initial stages, most cases of ovarian cancer are diagnosed at an advanced stage [2]. Surgery, platinum-based chemotherapy and targeted therapy are common treatment options for ovarian cancer. However, the mortality rate due to ovarian cancer has not significantly declined over the last four decades. The occurrence of chemoresistance also contributes to the increased mortality of patients with ovarian cancer. Indeed, ovarian cancer cells have an increased antioxidant capacity and express membrane transporters that can pump out the drug from the cells [3]. Therefore, in-depth characterization of the pathogenetic mechanisms of ovarian cancer and identification of the associated molecular regulators is imperative to improve the treatment of ovarian cancer.

GTPase-activating proteins (GAPs) are regulators of GTPase proteins and other domains, which directly or indirectly contribute to many cell functions and processes, including programmed cell death (PCD) [4]. Altered expression level of GAPs is associated with many types of cancer. For instance, ARHGAP5 and ARHGAP11A were

found to be upregulated in metastatic colorectal cancers and gastrointestinal cancers, respectively [5,6]. Of direct relevance to our work, Luo *et al.* [7] reported downregulation of a GAP named ARHGAP10 in ovarian cancer, while its overexpression was found to inhibit cancer cell adhesion, migration, invasion, and viability. Although their study showed that the anticancer effects of ARHGAP10 were mediated via inhibition of Cdc42 and activation of cancer cell apoptosis, the potential contribution of other signaling pathways and cell death mechanisms cannot be ruled out. Indeed, in the above-cited study, overexpression of ARHGAP10 was found to down-regulate PCNA, PARP1, and PARP2 [7], all of which are associated with another type of PCD—ferroptosis [8–10], which is also a newly emerging approach for cancer therapy [11].

Butyrate is a fatty acid that can regulate multiple cell cycle protein including GAPs [12]. Due to the inhibitory effect of butyrate on the proliferation of cancer cells (e.g., colorectal and gastric cancer [12,13]), it was suggested as a promising medication supplement for cancer treatment. Although the most acknowledged mechanism of butyrate-induced tumor inhibition is via the mitochondrial apoptosis pathway [14], we noticed that butyrate can also trigger ferroptosis in certain types of cells [15].



The above body of evidence prompted us to study whether the cancer-inhibitory effects of ARHGAP10 and butyrate are in part due to ferroptosis. We found that ARHGAP10 directly facilitated ferroptosis of ovarian cancer cells, which inhibited cancer cell viability and tumor growth in mice. Treatment of ovarian cancer cells with sodium butyrate (SB) greatly elevated the transcription level of ARHGAP10, which in turn facilitated ferroptosis. These results indicated a direct contribution of both ARHGAP10 and butyrate to the ferroptosis of ovarian cancer cells and revealed a previously undiscovered signaling pathway between these two molecules, with SB transcriptionally regulating ARHGAP10. Overall, our study unraveled the ferroptosis induced by SB and ARHGAP10, which expands our understanding of cancer pathology and may inspire novel anticancer therapeutic strategies.

2. Material and Methods

2.1 Cell Culture and Processing

OVCAR3 and A2780 human ovarian cancer cell lines were acquired from the Chinese Type Culture Collection, Chinese Academy of Sciences. The cells were cultured at 37 °C and 5% CO₂, in Roswell Park Memorial Institute (RPMI) 1640 medium (Life Technologies, Grand Island, NY, USA) supplemented with 10% fetal bovine serum (Gibco, Grand Island, NY, USA), 100 U/mL penicillin sodium, and 100 mg/mL streptomycin sulfate. All the cell lines were authenticated by short tandem repeat and were confirmed negative for mycoplasma contamination (Mycoalert Mycoplasma Detection Kit, Lonza, Monteggio, Switzerland).

The sequence of shRNA targeting ARHGAP10 (shARHGAP10) was GGTTTACAATTATCAGAAA. The shRNA was included in pLKO.1 lentiviral vector (Addgene, Watertown, MA, USA). Lentiviral constructs of pLKO.1-scramble shRNA (shNC), pLKO.1-shARHGAP10, pLVX-Puro empty vector (Clontech, Palo Alto, CA, USA), or pLVX-Puro-ARHGAP10 were co-transfected with viral packaging plasmids (psPAX2 and pMD2.G) into 293T cells. The viral supernatant was harvested after 48 h and filtered. A2780 cells were infected with pLVX-Puro-ARHGAP10 lentivirus while OVCAR3 cells were infected with pLKO.1-shARHGAP10 lentivirus with 8 µg/mL polybrene. Stable pools were obtained with 0.5 µg/mL puromycin (Sigma, St. Louis, MO, USA).

2.2 Cell viability Assay

A2780 cells infected with pLVX-Puro-ARHGAP10 lentivirus were treated with or without 25 µM apoptosis inhibitor zVAD-fmk, 20 µM necroptosis inhibitor necrostatin-1 (Nec-1), or 5 µM ferroptosis inhibitor ferrostatin-1 (Fer; all from Selleck, Shanghai, China). Another set of A2780 cells was infected with pLVX-Puro-ARHGAP10 lentivirus and/or treated with 5 µM Fer-1.

OVCAR3 cells were infected with pLKO.1-shARHGAP10 lentivirus and/or treated with 1 µg/mL

RSL3 (Selleck, Shanghai, China). Another set of OVCAR3 cells was treated with 0.5 mM sodium butyrate with or without pLKO.1-shARHGAP10 lentivirus infection. Cell Counting Kit-8 (CCK-8) Assay Kit (Dojindo Lab, Kumamoto, Japan) was then used to measure cell viability in 96-well plates (2 × 10³ cells per well). At 0, 12, 24, and 48 h, CCK-8 solution was added, and optical density values were measured using a microplate reader (Bio-Rad, Richmond, CA, USA) after 1 h.

2.3 Lactate Dehydrogenase (LDH) Release Cell Death Assay

A2780 cells infected with pLVX-Puro-ARHGAP10 lentivirus were treated with or without 25 µM zVAD-fmk, 20 µM Nec-1, or 5 µM Fer-1. Cell death rate was determined using the LDH cytotoxicity assay kit (Beyotime Biotechnology, Shanghai, China; C10016), as per the manufacturer's instructions, and calculated as previously described [16].

2.4 Lipid Reactive Oxygen Species (ROS) and Iron Content Measurements

Cells (3 × 10⁵ per well) were cultured overnight. A2780 cells were infected with pLVX-Puro-ARHGAP10 lentivirus and/or treated with 5 µM Fer-1. OVCAR3 cells were infected with pLKO.1-shARHGAP10 lentivirus and/or treated with 1 µg/mL RSL3. Another set of OVCAR3 cells was treated with 0.5 mM SB with or without pLKO.1-shARHGAP10 lentivirus infection. At 48 h, C11-BODIPY (10 µM; Thermo Fisher Scientific, Waltham, MA, USA) was added to the cell suspension and incubated for 30 min at 37 °C in the dark. After washing twice with PBS, the fluorescence intensity of the cells was measured by a CytoFLEX flow cytometer (Beckman Coulter, Miami, FL, USA). The Iron Assay Kit (Abcam, Waltham, MA, USA; ab83366) was used to detect Fe²⁺ content, as per the manufacturer's instructions.

2.5 RNA Isolation and Quantitative Real-time Polymerase Chain Reaction (RT-PCR)

Total RNA was extracted from cells using Trizol reagent (Invitrogen, Carlsbad, CA, USA). The mRNA levels of ARHGAP10 were determined by quantitative RT-PCR using GAPDH as a control. The primer sequences used were as follows: ARHGAP10, 5'-AAGGAGGACACCCCTACCAG-3' and 5'-GGATGCCAGTCTCCAAAG-3'; GAPDH, 5'-TCCCATCACCATCTTCCAGG-3' and 5'-GATGACCCCTTTGGCTCCC-3'. Specific product amplification was verified by dissociation curve analysis. The foldchange for target genes normalized by internal control was determined by the 2^{-ΔΔCT} formula.

2.6 Antibodies and Western Blotting

Cells were lysed in ice-cold radioimmunoprecipitation assay buffer (50 mM Tris-HCl [pH 7.5], 150 mM NaCl,

Table 1. Antibodies used for Western blot.

Antibody name	Source	Cat. no	Dilution
ARHGAP10	Proteintech Group	55139-1-AP	1:1000
GPX4	Abcam	ab125066	1:1000
PTGS2	Abcam	ab179800	1:1000
H3K9ac	Abcam	ab32129	1:500
β -actin	Abcam	ab8226	1:1000
horseradish peroxidase-conjugated goat anti- rabbit IgG	ZSGB-BIO	ZB-2301	1:5000
horseradish peroxidase-conjugated goat anti-mouse IgG	ZSGB-BIO	ZB-2305	1:5000

1% Triton X-100, 0.5% Na-deoxycholate) containing protease inhibitors. Protein concentration was measured using a BCA protein assay kit (Thermo Fisher Scientific). Equal amounts of cell lysates were separated on sodium dodecyl-sulfate polyacrylamide gel electrophoresis (SDS-PAGE) gels, transferred to polyvinylidene fluoride (PVDF) membranes, and analyzed by Western blotting using an enhanced chemiluminescence system (Bio-Rad, Richmond, CA, USA). The antibodies used are listed in Table 1. Band intensities were analyzed using Image J (NIH, Bethesda, MD, USA) and normalized to β -actin.

2.7 Chromatin Immunoprecipitation (ChIP) Assay

OVCAR3 cells were treated with 0.5 mM sodium butyrate or left untreated for 48 h, and then fixed with 1% formaldehyde. The fixed cells were sonicated for chromatin fragmentation. The chromatin solutions were then incubated overnight with anti-H3K9ac (Cell Signaling Technology, Danvers, MA, USA; 9649) or control IgG antibody (Cell Signaling Technology; 3900) at 4 °C. H3K9ac binding in the ARHGAP10 promoter region was quantified by PCR using the following ARHGAP10 promoter primers: 5'-AAGAGCCCCCTGTGCGAGTT-3' (Forward) and 5'-GGCGGGCGACATAACTCT-3' (Reverse).

2.8 In Vivo Tumorigenicity Assay

Athymic Balb/c nude mice (age: 5 weeks) were acquired from the Slac Laboratory Animal Co. Ltd. (Shanghai, China) and housed in a pathogen-free animal facility. Mice were randomly assigned to control or experimental groups (6 per group). A2780 cells infected with pLVX-Puro-ARHGAP10 lentivirus were injected intraperitoneally into the flank of each mouse ($2 \times 10^6/0.1$ mL). Injection of Fer-1 (5 mg/kg) was administered twice a week. Tumor volume was estimated once every 3 days: volume = $1/2 \times \text{length} \times \text{width}^2$. On day 35, the mice were sacrificed by cervical dislocation after an intraperitoneal injection of sodium pentobarbital (30 mg/kg; Sigma-Aldrich, St. Louis, MO, USA). The animal study was carried out in accordance with the guidelines approved by the Animal Experimentation Ethics Committee of Shanghai Pudong Hospital, Fudan University Pudong Medical Center [(2021)No.(QKW-02)].

2.9 Immunofluorescence Microscopy

After fixation and permeabilization, the tissues collected from the xenograft tumor were incubated with 1% bovine serum albumin for 30 min for blocking and then with anti-Ki67 (Abcam; ab243878) and Alexa Fluor 488-labeled Goat Anti-Mouse IgG (H + L) (Beyotime Biotechnology; A0423). DAPI (Beyotime Biotechnology; C1002) labeling was used for nuclear staining. Then, positively stained cells were visualized using a confocal laser scanning microscope (Leica Microsystems, Inc., Wetzlar, Germany).

2.10 Statistical Analysis

All experiments were conducted in triplicate. Data were expressed as mean \pm standard deviation (SD). All statistical analyses were performed using GraphPad Prism 8.4.2 (GraphPad Software, San Diego, CA, USA). Differences between two groups were assessed for statistical significance using the Students *t*-test, while ANOVA was used for multi-group comparisons. *p* values < 0.05 were considered indicative of statistical significance.

3. Results

3.1 ARHGAP10 Promotes Ferroptosis in Ovarian Cancer Cells

To understand the effects of ARHGAP10 on ovarian cancer, we first used pLVX-Puro-ARHGAP10 lentivirus to induce the overexpression of ARHGAP10. A2780 cell line was used as an *in vitro* cell model of human ovarian cancer. After infection with pLVX-Puro-ARHGAP10 lentivirus, the A2780 cells showed much higher mRNA and protein expression of ARHGAP10 compared with non-infected cells (Control) or cell infected with empty lentivirus (Vector) (Fig. 1A,B), confirming the success of the infection.

Consistent with a previous study [7], our results showed that ARHGAP10 overexpression caused a significant decrease in cell viability (Fig. 1C) and an increase in cell death (Fig. 1D). To determine the cause of ARHGAP10 overexpression-induced cell death, several cell death inhibitors were tested. Ferroptosis inhibitor Fer-1 markedly inhibited the ARHGAP10 overexpression-induced cell viability decrease and cell death. However, apoptosis inhibitor zVAD-fmk only slightly inhibited ARHGAP6 overexpression-induced cell viability decrease and cell death (Fig. 1C,D). To further examine

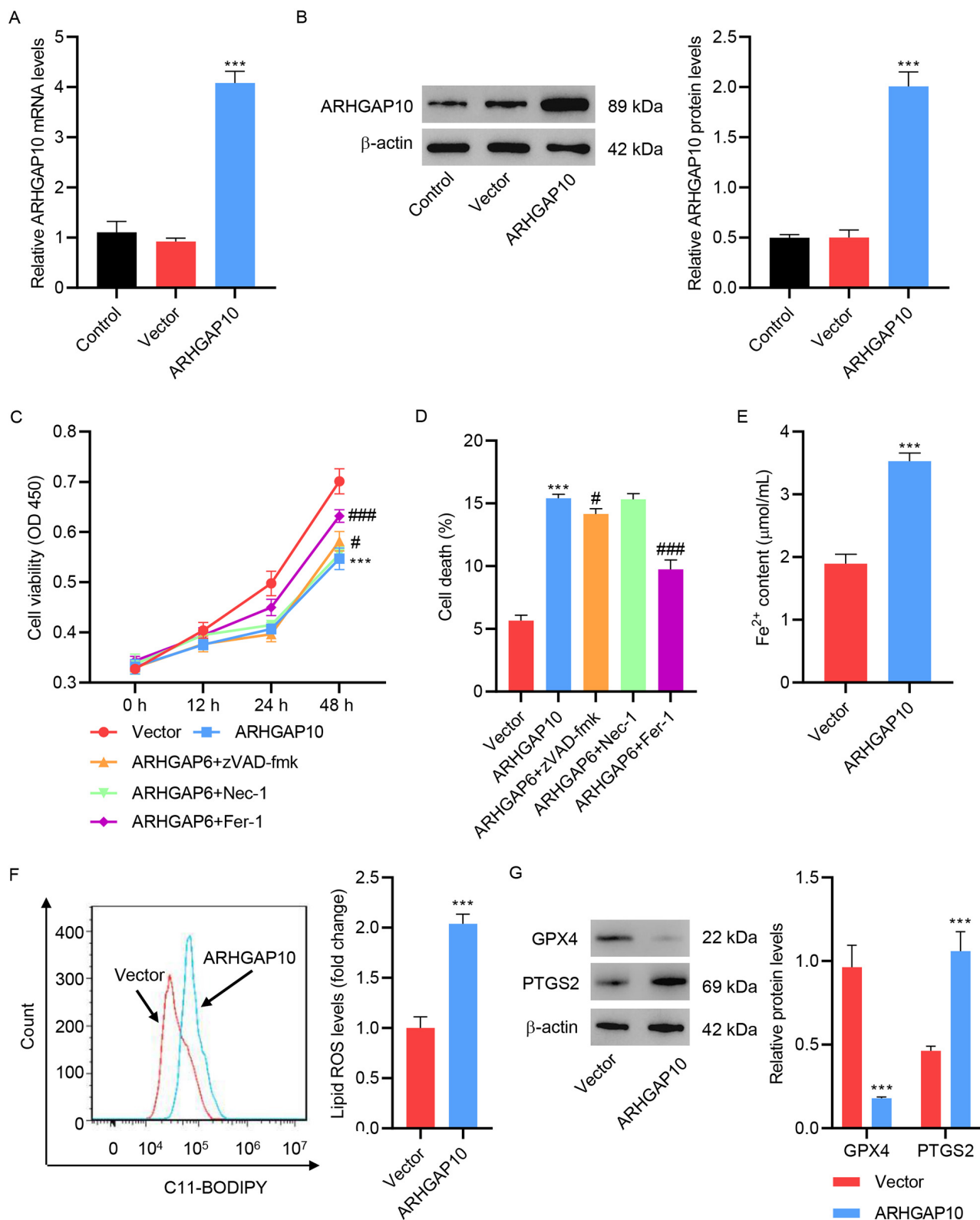


Fig. 1. ARHGAP10 overexpression promotes A2780 cell ferroptosis. (A) mRNA and (B) protein levels of ARHGAP10 in A2780 cells infected with pLVX-Puro-ARHGAP10 lentivirus or control lentivirus ($n = 3$). A2780 cells were infected with pLVX-Puro-ARHGAP10 lentivirus and treated with 25 μM apoptosis inhibitor zVAD-fmk, 20 μM necroptosis inhibitor Nec-1, or 10 μM ferroptosis inhibitor Fer-1, and the (C) cell viability and (D) cell death were determined ($n = 3$). The (E) Fe^{2+} content, (F) lipid reactive oxygen species (ROS), and (G) expression of GPX4 and PTGS2 in A2780 cells infected with pLVX-Puro-ARHGAP10 lentivirus or control lentivirus ($n = 3$). *** $p < 0.001$ vs. vector. # $p < 0.05$, ### $p < 0.001$ vs. ARHGAP10.

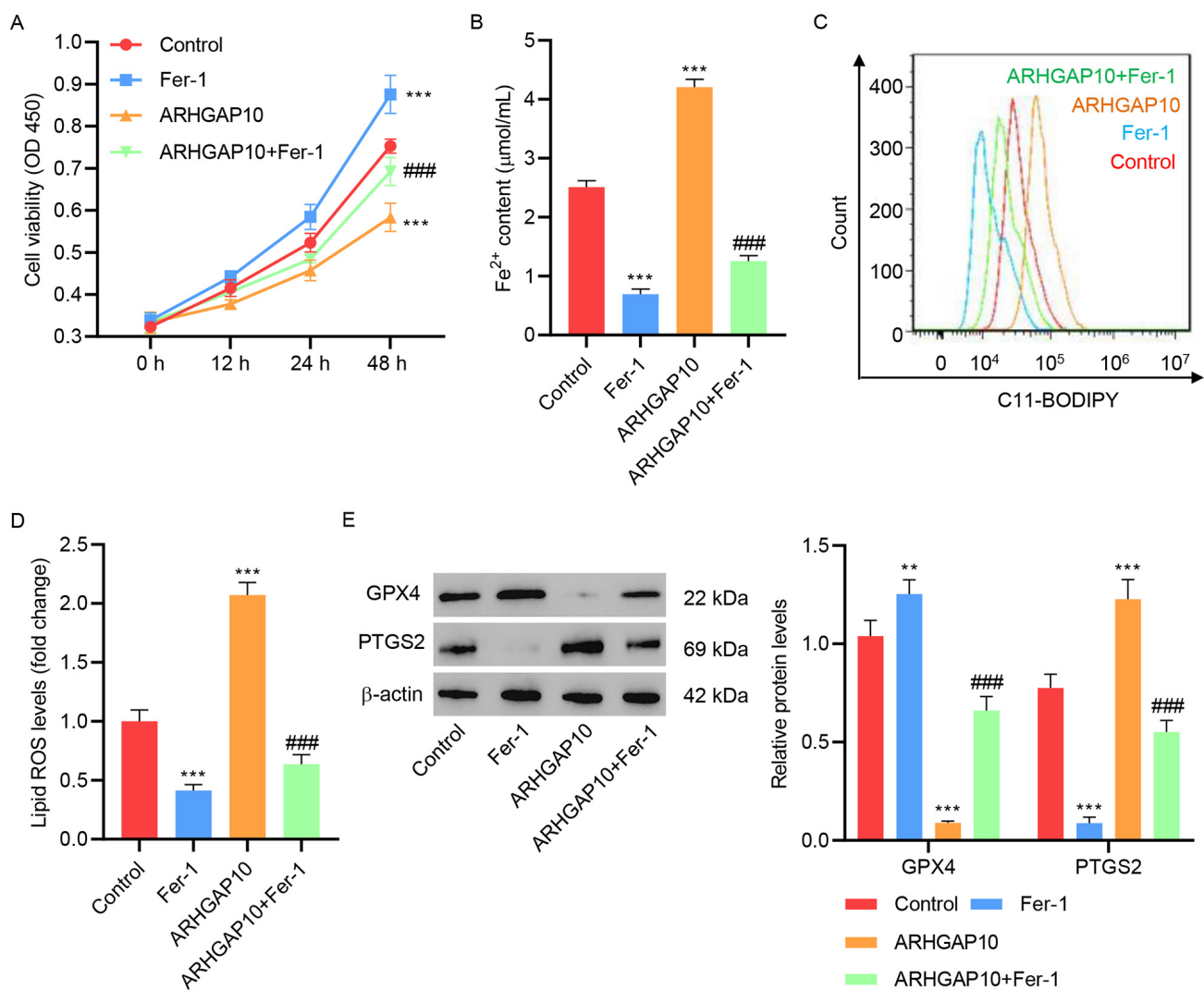


Fig. 2. Fer-1 inhibits ARHGAP10 overexpression-induced ferroptosis in A2780 cells. (A) Cell viability, (B) Fe²⁺ content, (C,D) lipid ROS, and (E) expression of GPX4 and PTGS2 in A2780 cells infected with pLVX-Puro-ARHGAP10 lentivirus and treated with Fer-1 (n = 3). **p < 0.01, ***p < 0.001 vs. control. ####p < 0.001 vs. ARHGAP10.

the effects of ferroptosis on ARHGAP10 overexpression-mediated cell death, Fe²⁺ content, and lipid ROS levels were measured. Fe²⁺ content (Fig. 1E) and lipid ROS levels (Fig. 1F) were significantly increased in ARHGAP10-overexpressing A2780 cells, suggesting the intensification of ferroptosis, an iron-dependent PCD pathway distinctive from apoptosis, necrosis, and autophagy, characterized by the accumulation of lipid-based ROS [17]. Therefore, we focused on ferroptosis by measuring the expression level of two proteins indicative of ferroptosis, glutathione peroxidase 4 (GPX4), a protective protein that prevents lipid peroxidation and ferroptosis [18], and Prostaglandin-Endoperoxide Synthase 2 (PTGS2), a well-established biomarker of ferroptosis [19]. As shown by the Western blot assay, ARHGAP10 overexpression substantially decreased the expression of GPX4 and increased that of PTGS2 (Fig. 1G). These results consistently indicated that ARHGAP10 overexpression triggered ferroptosis in ovarian cancer cells.

3.2 Fer-1 Inhibits ARHGAP10-Induced Ferroptosis

To further confirm the triggering of ferroptosis by ARHGAP10 overexpression, we tested the effect of Fer-1. Both in the absence and presence of ARHGAP10 overexpression, treatment with Fer-1 significantly increased cell viability (Fig. 2A), and decreased the Fe²⁺ content (Fig. 2B) and lipid ROS levels (Fig. 2C,D), indicating protection from cell death. Importantly, Fer-1 upregulated the expression of GPX4 and down-regulated that of PTGS2 in uninfected cells; furthermore, it reversed ARHGAP10 overexpression-induced decrease of GPX4 expression and enhancement of PTGS2 expression, to the level approximating that in the uninfected untreated control cells (Fig. 2E). Collectively, these results indicated that ARHGAP10 overexpression-induced ferroptosis in A2780 cells, which was suppressed by Fer-1.

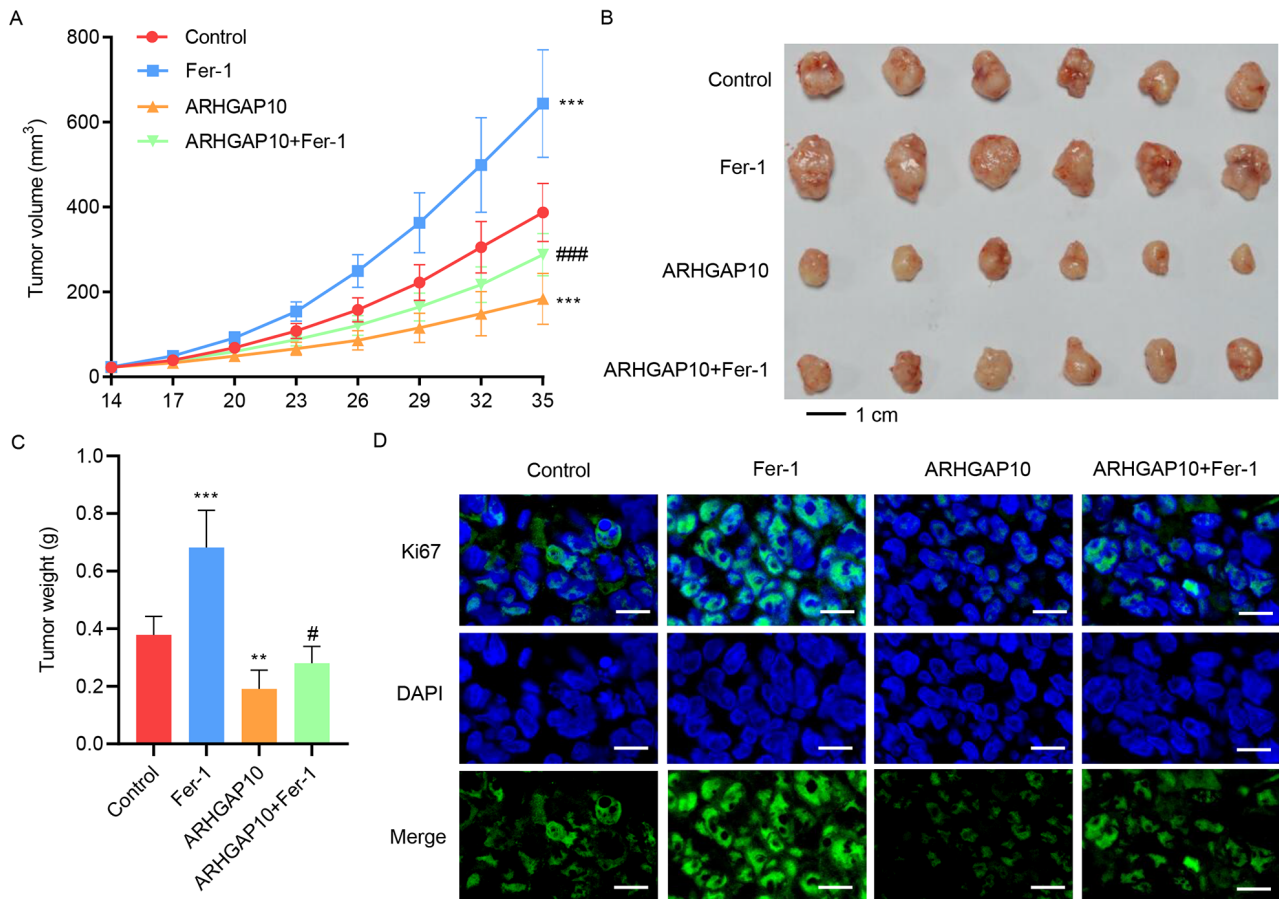


Fig. 3. Fer-1 inhibits ARHGAP10 overexpression-induced suppression of tumor growth *in vivo*. Mice injected with A2780 cells were treated with Fer-1 for 35 days. Tumor (A) volume, (B,C) weight, and (D) Ki67 immunofluorescence staining (scale bar, 20 μ m) were quantified (n = 6). ** p < 0.01, *** p < 0.001 vs. control. # p < 0.05, ### p < 0.001 vs. ARHGAP10.

3.3 Fer-1 Inhibits ARHGAP10-Induced Suppression of Tumor Growth

In a previous study, ARHGAP10 was found to suppress tumor growth [7], which was argued to be contributed by apoptosis. However, other molecular mechanisms may also be involved in contributing to this effect. Based on our above results which showed that ARHGAP10 triggers ferroptosis in cancer cells, we hypothesized that it also contributes to tumor suppression.

To test our hypothesis, mice were injected with A2780 cells with or without ARHGAP10 overexpression to induce tumor development. Some of the mice in both groups were then treated with Fer-1 for 35 days, while the rest were left untreated. The development of tumors in each mouse was monitored for 35 days. Compared to the control group, tumors in mice treated with Fer-1 were larger and heavier, suggesting that ferroptosis is indeed a regulator of ovarian tumor growth (Fig. 3A–C). Notably, whereas ARHGAP10 overexpression significantly decreased tumor size and weight, these effects were reversed by Fer-1 (Fig. 3A–C).

We also looked at immunofluorescence staining of Ki67, a commonly used biomarker of cell proliferation [20],

in the xenograft tumor tissue. While Fer-1 greatly increased the signal intensity of Ki67 in the tumor cells, suggesting higher viability and greater proliferation, the signal intensity was drastically decreased by ARHGAP10 overexpression, and was restored to a level comparable to the control group by the copresence of ARHGAP10 overexpression and Fer-1 (Fig. 3D). These results indicated that ARHGAP10-induced suppression of tumor growth was in part via the ferroptosis pathway, which can be inhibited by Fer-1.

3.4 RSL3 Inhibits ARHGAP10 Silencing-Induced Suppression of Ferroptosis

ARHGAP10 silencing is another way to re-confirm the observed relation between ARHGAP10 and ferroptosis. A shRNA targeting ARHGAP10 (shARHGAP10) was developed for this purpose and used to construct the pLKO.1-shARHGAP10 lentivirus. Infection of OVCAR3 cells with the control lentivirus (shNC) had no effect on the mRNA and protein expression levels of ARHGAP10. However, OVCAR3 cells infected with pLKO.1-shARHGAP10 manifested much lower mRNA and protein expression levels of ARHGAP10, confirming the specificity of pLKO.1-

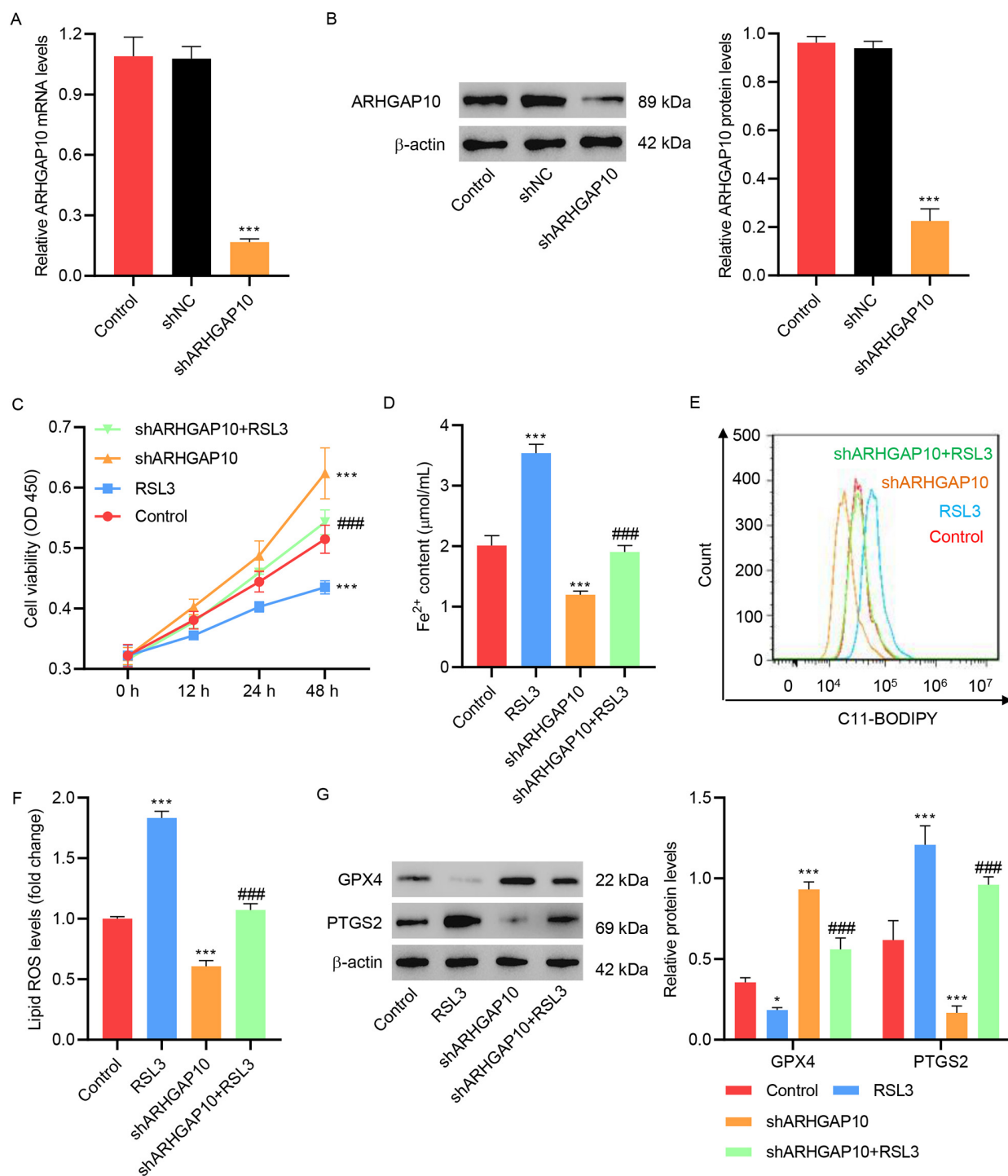


Fig. 4. RSL3 inhibits ARHGAP10 silencing-induced suppression of ferroptosis in OVCAR3 cells. (A) mRNA and (B) protein levels of ARHGAP10 in OVCAR3 cells infected with pLKO.1-shARHGAP10 lentivirus or control lentivirus ($n = 3$). (C) Cell viability, (D) Fe²⁺ content, (E,F), lipid ROS, and (G) expression of GPX4 and PTGS2 in OVCAR3 cells infected with pLKO.1-shARHGAP10 lentivirus and/or treated with RSL3 ($n = 3$). * $p < 0.05$, *** $p < 0.001$ vs. control. ### $p < 0.001$ vs. shARHGAP10.

shARHGAP10 in ARHGAP10 silencing (Fig. 4A,B). Silencing of ARHGAP10 significantly increased cell viability (Fig. 4C), Fe²⁺ content (Fig. 4D), and lowered lipid ROS level (Fig. 4E,F), as well as increased and decreased the expression of GPX4 and PTGS2, respectively (Fig. 4G). These findings are consistent with our above findings, indicating suppression of ferroptosis.

RSL3 is a facilitator of cell ferroptosis, which has been shown to inactivate GPX4 and stimulate ROS production in cancer cells [21,22]. Here, we showed that RSL3 decreased the viability of OVCAR3 cells, increased the lipid ROS level, and decreased and increased the expression of GPX4 and PTGS2, respectively (Fig. 4C–G). Treatment of OVCAR3 cells with RSL3 reversed the effect of ARHGAP10

silencing so that the cell viability level, lipid ROS level as well as GPX4 and PTGS2 expression levels were at an intermediate level between the ARHGAP10-silenced group and RSL3-treated group (Fig. 4C–G).

3.5 SB Promotes Ovarian Cancer Cell Ferroptosis by Transcriptional Regulation of ARHGAP10

Lastly, we investigated the potential relation of SB with ARHGAP10 in ferroptosis. Treatment of ovarian cancer cells with SB greatly increased the mRNA and protein expression levels of ARHGAP10 (Fig. 5A,B). SB also increased the expression level of H3K9ac, a marker of transcriptional activation of genes (Fig. 5B). This suggested that SB may enhance the expression of ARHGAP10 by regulating the transcription of its encoding gene. The results of the ChIP assay showed that SB can increase the binding of H3K9ac to the promoter region of ARHGAP10 (Fig. 5C,D).

Consistent with the above finding, we further found that SB significantly decreased the viability of OVCAR3 cells (Fig. 5E), increased the Fe²⁺ content (Fig. 5F) and level of lipid ROS (Fig. 5G), as well as decreased and increased the expression level of GPX4 and PTGS2, respectively (Fig. 5H). All these findings indicate the role of SB in inducing ferroptosis. However, silencing the ARHGAP10 mRNA with shARHGAP10 abrogated all the above effects of SB, bringing the cell viability and lipid ROS, GPX4, and PTGS2 levels back to the levels comparable to the control condition (Fig. 5E–H). These results strongly suggested that transcriptional regulation of ARHGAP10 is the only mechanism by which SB promotes ferroptosis in ovarian cancer cells.

4. Discussion

A key bottleneck in current cancer treatment, including conventional approaches like chemotherapy, or relatively novel ones like immunotherapy, is the development of resistance against these therapies [23]. Previous studies have found that cancer cells can undergo ferroptosis, a new type of PCD distinct from apoptosis, necrosis, or autophagy [24], in response to radiotherapy, chemotherapy, and immunotherapy [23], suggesting that activating cell ferroptosis may serve as a promising strategy to increase the efficacy of anticancer treatment. Of relevance to this work, ferroptosis has been proposed as an advanced strategy for treating ovarian cancer. For instance, ferroptosis inducers were found to increase the sensitivity of BRCA-proficient ovarian cancer cells and xenografts to pharmacologic PARP inhibitors [10]. In the present study, ARHGAP10 was found to facilitate ovarian cancer cell ferroptosis, which is transcriptionally regulated by SB. Altogether, these results highlight ARHGAP10 as a potential target for drug development against ovarian cancer and delineate the underlying mechanism by which SB induces ferroptosis.

Since its discovery in 2012 [25], ferroptosis is known to be mediated by at least eight major pathways: the glutathione-GPX4 pathway, NADPH-FSP1-CoQ10 path-

way, P53-mediated lipoxygenase and iPLA2 β pathway, iNOs/NO pathway, DHODH pathway, GCH1/BH4 pathway, Ferritin and prominin2 pathway, and SREBP1-SCD1-MUFA pathway [26]. Among them, the glutathione-GPX4 pathway was discovered first, wherein GPX4 inhibits ferroptosis by down-regulating lipid peroxide production [27]. The latter seven pathways are all GPX4-independent pathways. In this work, ARHGAP10 was found to decrease the expression of GPX4, indicating that ARHGAP10 is associated with a GPX4-dependent pathway, presumably the glutathione-GPX4 pathway. However, whether it also interacts with the other seven pathways remains unclear. Furthermore, RSL3 was found to reverse the anti-ferroptotic effects of ARHGAP10 silencing. However, it is not clear whether RSL3 targets signaling molecules downstream of ARHGAP10, or it is involved in another signaling pathway that is independent of ARHGAP10, or whether both the above mechanisms coexist. Answering the above-unsolved questions is important to figure out the molecular mechanism(s) of ARHGAP10-induced ferroptosis.

Interestingly, ARHGAP10 was only reported to enhance apoptosis in ovarian cancer cells, which was believed to be the sole mechanism of its induced tumor suppression [7]. Our work provides a paradigm shift by discovering a second mechanism that is based on ferroptosis. This suggests that targeting ARHGAP10 can have at least bifold effects for treating ovarian cancer because it can concurrently facilitate both apoptosis and ferroptosis. Furthermore, our discovery opens several future directions of research. First, it is intriguing to ask whether ARHGAP10 is also associated with other types of PCD. In addition, its relationship with necrosis has not been discussed before. Figuring out the exact contributions of ARHGAP10 to PCD will enable an in-depth understanding of its mechanisms of action and facilitate its targeting for therapeutic purposes. Second, different types of PCD can have synergistic effects on each other to achieve stronger effects. For example, autophagy can facilitate ferroptosis by degrading ferritin [28]. We therefore, are curious whether the apoptosis and ferroptosis signaling pathways downstream of ARHGAP10 have any overlapping or mutual effects. Lastly, recent studies have shown that ARHGAP10 is associated with various cancers, such as head and neck squamous cell carcinoma [29], gliomas [30], and prostate cancer [31]. It would be extremely meaningful to expand our study and explore whether ARHGAP10 can also facilitate ferroptosis in other types of cancer.

SB has shown great potential in cancer treatment [12,13,32]. Similar to ARHGAP10, the tumor inhibitory effect of SB is also believed to be due to its proapoptotic effects. Specifically, by increasing the expression of DAPK, SB potentially increases the expression of several cell-cycle inhibitors (e.g., CDKN1A, CDKN1B) and the activity of several proapoptotic genes (e.g., *BAX*, *BAK*, and *BIK*) [13]; it also down-regulates certain cancer-facilitating molecules (e.g., Thioredoxin-1) [33]. Here we show that ferroptosis may also contribute to SB-induced tumor suppression,

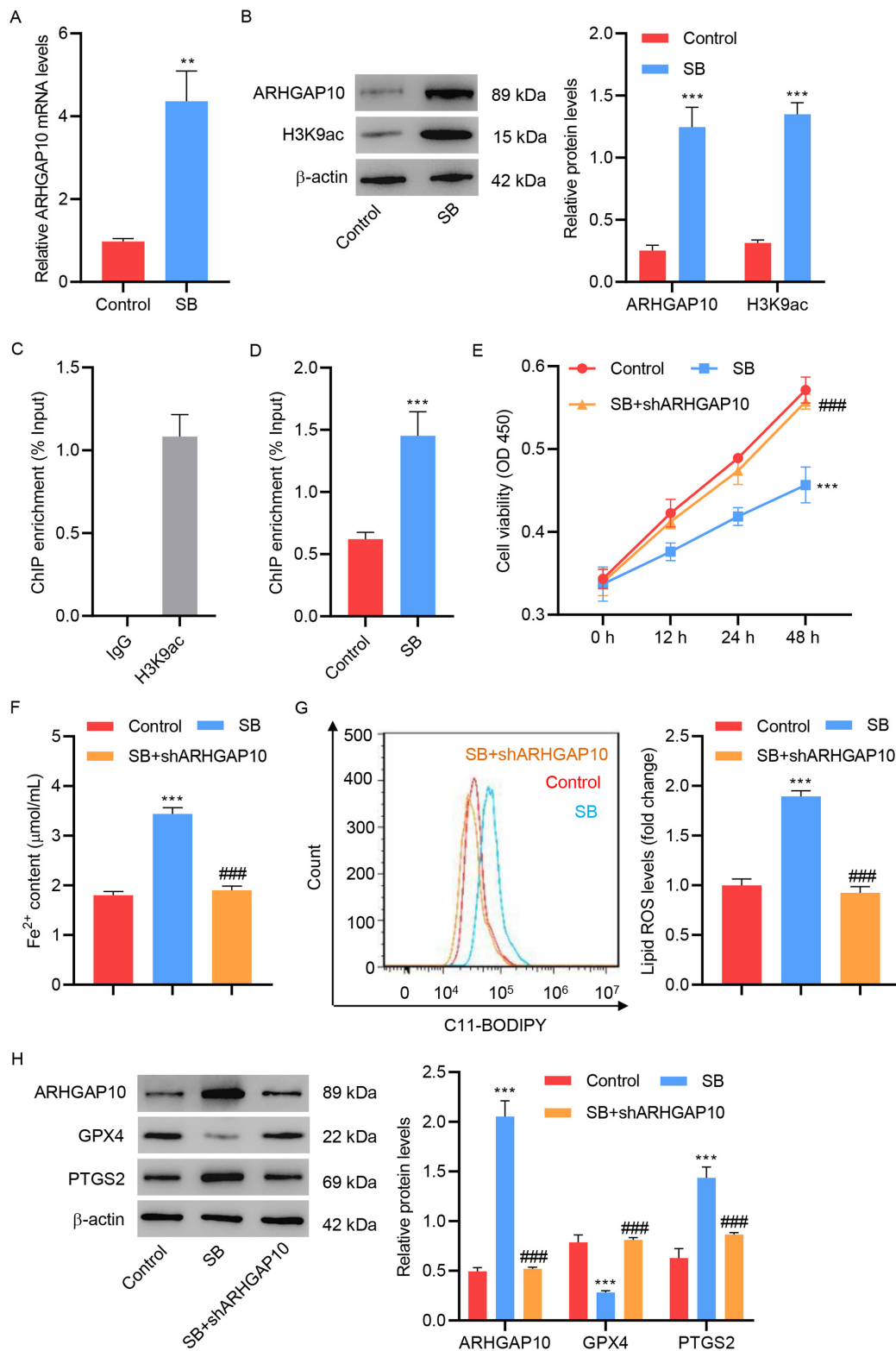


Fig. 5. Sodium butyrate promotes OVCAR3 cell ferroptosis by transcriptional regulation of ARHGAP10. (A) mRNA levels of ARHGAP10 and (B) protein levels of ARHGAP10 and H3K9ac in OVCAR3 cells treated with sodium butyrate (SB) (n = 3). (C) Chromatin from OVCAR3 cells was immunoprecipitated using control IgG or H3K9ac antibody, and the results were measured by quantitative PCR (n = 3). (D) Chromatin from OVCAR3 cells with or without SB treatment were immunoprecipitated using the H3K9ac antibody, and the results were measured by quantitative PCR (n = 3). (E) Cell viability, (F) Fe²⁺ content, (G) lipid ROS, and (H) expression of ARHGAP10, GPX4, and PTGS2 in OVCAR3 cells treated with SB were infected with or without pLKO.1-shARHGAP10 lentivirus (n = 3). ***p* < 0.01, ****p* < 0.001 vs. control. ###*p* < 0.001 vs. SB.

which emphasizes the therapeutic potential of SB. Furthermore, by pinpointing ARHGAP10 as a necessary signaling molecule mediating the effect of SB on ferroptosis, our findings seem to suggest a pivotal role of ARHGAP10 in the signaling network of ferroptosis, which would require future investigations.

5. Conclusions

In this study, ARHGAP10 was found to promote ferroptosis of ovarian cancer cells via a GPX4-dependent pathway to suppress tumor development. Furthermore, SB was found to regulate the transcription of ARHGAP10, thereby also contributing to ovarian cancer cell ferroptosis. To the best of our knowledge, this is the first study to report ferroptosis-related functions of SB and ARHGAP10. Our study expands our current understanding of the anti-tumor effects of SB and ARHGAP10 and emphasizes the SB/ARHGAP10/GPX4 signaling pathway as a promising therapeutic target in the context of ovarian cancer.

Availability of Data and Materials

The datasets used and/or analyzed during the present study are available from the corresponding author on reasonable request.

Author Contributions

Conceptualization: HK and JS; Methodology: JS, JH, XS, HH, LC and ZZ; Formal analysis and investigation: JH, XS, YS and XZ; Writing-original draft preparation: HK; Writing-review and editing: LC and YS; Funding acquisition: YS; Supervision: XZ, LC and YS. All authors contributed to editorial changes in the manuscript. All authors read and approved the final manuscript. All authors have participated sufficiently in the work and agreed to be accountable for all aspects of the work.

Ethics Approval and Consent to Participate

All experimental procedures were performed in accordance with the Guidelines for the Animal Experimentation Ethics Committee of Shanghai Pudong Hospital, Fudan University Pudong Medical Center [(2021)No.(QKW-02)].

Acknowledgment

Not applicable.

Funding

This study was funded by the Science and Technology Development Fund of Shanghai Pudong (PKJ2021-Y36) and Key Specialty Construction Project of Pudong Health and Family (PWZzk2022-21) and supported by the Project of Key Medical Specialty and Treatment Center of Pudong Hospital of Fudan University (Tszb2023-03).

Conflict of Interest

The authors declare no conflict of interest.

References

- [1] Torre LA, Bray F, Siegel RL, Ferlay J, Lortet-Tieulent J, Jemal A. Global cancer statistics, 2012. *CA: A Cancer Journal for Clinicians*. 2015; 65: 87–108.
- [2] Matulonis UA, Sood AK, Fallowfield L, Howitt BE, Sehouli J, Karlan BY. Ovarian cancer. *Nature Reviews. Disease Primers*. 2016; 2: 16061.
- [3] Tossetta G, Fantone S, Goteri G, Giannubilo SR, Ciavattini A, Marzioni D. The Role of NQO1 in Ovarian Cancer. *International Journal of Molecular Sciences*. 2023; 24: 7839.
- [4] He H, Huang J, Wu S, Jiang S, Liang L, Liu Y, *et al.* The roles of GTPase-activating proteins in regulated cell death and tumor immunity. *Journal of Hematology & Oncology*. 2021; 14: 171.
- [5] Tian T, Chen ZH, Zheng Z, Liu Y, Zhao Q, Liu Y, *et al.* Investigation of the role and mechanism of ARHGAP5-mediated colorectal cancer metastasis. *Theranostics*. 2020; 10: 5998–6010.
- [6] Fan B, Ji K, Bu Z, Zhang J, Yang H, Li J, *et al.* ARHGAP11A Is a Prognostic Biomarker and Correlated With Immune Infiltrates in Gastric Cancer. *Frontiers in Molecular Biosciences*. 2021; 8: 720645.
- [7] Luo N, Guo J, Chen L, Yang W, Qu X, Cheng Z. ARHGAP10, downregulated in ovarian cancer, suppresses tumorigenicity of ovarian cancer cells. *Cell Death & Disease*. 2016; 7: e2157.
- [8] Meng Q, Xu Y, Ling X, Liu H, Ding S, Wu H, *et al.* Role of ferroptosis-related genes in coronary atherosclerosis and identification of key genes: integration of bioinformatics analysis and experimental validation. *BMC Cardiovascular Disorders*. 2022; 22: 339.
- [9] Li G, Lin SS, Yu ZL, Wu XH, Liu JW, Tu GH, *et al.* A PARP1 PROTAC as a novel strategy against PARP inhibitor resistance via promotion of ferroptosis in p53-positive breast cancer. *Biochemical Pharmacology*. 2022; 206: 115329.
- [10] Hong T, Lei G, Chen X, Li H, Zhang X, Wu N, *et al.* PARP inhibition promotes ferroptosis via repressing SLC7A11 and synergizes with ferroptosis inducers in BRCA-proficient ovarian cancer. *Redox Biology*. 2021; 42: 101928.
- [11] Zhang C, Liu X, Jin S, Chen Y, Guo R. Ferroptosis in cancer therapy: a novel approach to reversing drug resistance. *Molecular Cancer*. 2022; 21: 47.
- [12] Tan HT, Tan S, Lin Q, Lim TK, Hew CL, Chung MCM. Quantitative and temporal proteome analysis of butyrate-treated colorectal cancer cells. *Molecular & Cellular Proteomics: MCP*. 2008; 7: 1174–1185.
- [13] Li Y, He P, Liu Y, Qi M, Dong W. Combining Sodium Butyrate With Cisplatin Increases the Apoptosis of Gastric Cancer *In Vivo* and *In Vitro* via the Mitochondrial Apoptosis Pathway. *Frontiers in Pharmacology*. 2021; 12: 708093.
- [14] Salimi V, Shahsavari Z, Safizadeh B, Hosseini A, Khademian N, Tavakoli-Yaraki M. Sodium butyrate promotes apoptosis in breast cancer cells through reactive oxygen species (ROS) formation and mitochondrial impairment. *Lipids in Health and Disease*. 2017; 16: 208.
- [15] Zhao Y, Li J, Guo W, Li H, Lei L. Periodontitis-level butyrate-induced ferroptosis in periodontal ligament fibroblasts by activation of ferritinophagy. *Cell Death Discovery*. 2020; 6: 119.
- [16] Kuang H, Sun X, Liu Y, Tang M, Wei Y, Shi Y, *et al.* Palmitic acid-induced ferroptosis via CD36 activates ER stress to break calcium-iron balance in colon cancer cells. *The FEBS Journal*. 2023; 290: 3664–3687.
- [17] Yang L, Chen L, Chen T, Gao X, Xiong Y. The crosstalk between classic cell signaling pathways, non-coding RNAs and ferroptosis in drug resistance of tumors. *Cellular Signalling*. 2023; 102: 110538.
- [18] Seibt TM, Proneth B, Conrad M. Role of GPX4 in ferroptosis and its pharmacological implication. *Free Radical Biology & Medicine*. 2019; 133: 144–152.
- [19] Lei P, Bai T, Sun Y. Mechanisms of Ferroptosis and Relations

With Regulated Cell Death: A Review. *Frontiers in Physiology*. 2019; 10: 139.

- [20] Graefe C, Eichhorn L, Wurst P, Kleiner J, Heine A, Panetas I, *et al*. Optimized Ki-67 staining in murine cells: a tool to determine cell proliferation. *Molecular Biology Reports*. 2019; 46: 4631–4643.
- [21] Sui X, Zhang R, Liu S, Duan T, Zhai L, Zhang M, *et al*. RSL3 Drives Ferroptosis Through GPX4 Inactivation and ROS Production in Colorectal Cancer. *Frontiers in Pharmacology*. 2018; 9: 1371.
- [22] Li S, He Y, Chen K, Sun J, Zhang L, He Y, *et al*. RSL3 Drives Ferroptosis through NF- κ B Pathway Activation and GPX4 Depletion in Glioblastoma. *Oxidative Medicine and Cellular Longevity*. 2021; 2021: 2915019.
- [23] Zhao L, Zhou X, Xie F, Zhang L, Yan H, Huang J, *et al*. Ferroptosis in cancer and cancer immunotherapy. *Cancer Communications (London, England)*. 2022; 42: 88–116.
- [24] Li J, Cao F, Yin HL, Huang ZJ, Lin ZT, Mao N, *et al*. Ferroptosis: past, present and future. *Cell Death & Disease*. 2020; 11: 88.
- [25] Dixon SJ, Lemberg KM, Lamprecht MR, Skouta R, Zaitsev EM, Gleason CE, *et al*. Ferroptosis: an iron-dependent form of non-apoptotic cell death. *Cell*. 2012; 149: 1060–1072.
- [26] Ma T, Du J, Zhang Y, Wang Y, Wang B, Zhang T. GPX4-independent ferroptosis—a new strategy in disease’s therapy. *Cell Death Discovery*. 2022; 8: 434.
- [27] Chen X, Yu C, Kang R, Kroemer G, Tang D. Cellular degradation systems in ferroptosis. *Cell Death and Differentiation*. 2021; 28: 1135–1148.
- [28] Hou W, Xie Y, Song X, Sun X, Lotze MT, Zeh HJ, 3rd, *et al*. Autophagy promotes ferroptosis by degradation of ferritin. *Autophagy*. 2016; 12: 1425–1428.
- [29] Carles A, Millon R, Cromer A, Ganguli G, Lemaire F, Young J, *et al*. Head and neck squamous cell carcinoma transcriptome analysis by comprehensive validated differential display. *Oncogene*. 2006; 25: 1821–1831.
- [30] Bigarella CL, Borges L, Costa FF, Saad STO. ARHGAP21 modulates FAK activity and impairs glioblastoma cell migration. *Biochimica et Biophysica Acta*. 2009; 1793: 806–816.
- [31] Lazarini M, Traina F, Machado-Neto JA, Barcellos KSA, Moreira YB, Brandão MM, *et al*. ARHGAP21 is a RhoGAP for RhoA and RhoC with a role in proliferation and migration of prostate adenocarcinoma cells. *Biochimica et Biophysica Acta*. 2013; 1832: 365–374.
- [32] Chen M, Jiang W, Xiao C, Yang W, Qin Q, Mao A, *et al*. Sodium Butyrate Combined with Docetaxel for the Treatment of Lung Adenocarcinoma A549 Cells by Targeting Gli1. *OncoTargets and Therapy*. 2020; 13: 8861–8875.
- [33] Wang W, Fang D, Zhang H, Xue J, Wangchuk D, Du J, *et al*. Sodium Butyrate Selectively Kills Cancer Cells and Inhibits Migration in Colorectal Cancer by Targeting Thioredoxin-1. *OncoTargets and Therapy*. 2020; 13: 4691–4704.